QUANTITATIVE MRI MEASUREMENT OF BINDER DISTRIBUTIONS IN GREEN-STATE CERAMICS

N. Gopalsami, S.L. Dieckman, and W.A. Ellingson
Materials and Components Technology Division

R.E. Botto
Chemistry Division
Argonne National Laboratory
Argonne, IL 60439

H. Yeh
Garrett Ceramics Components Division
Allied Signal Aerospace Company
Torrance, CA 90509

INTRODUCTION

Development of reliable and improved structural ceramics for advanced heat engines and other applications requires process diagnostics and materials evaluation from powder preparation to green-body forming to final sintering. Injection molding is a promising processing method being developed for mass production of complex-shaped heat engine components such as turbochargers (rotors and stator vanes) and engine valves. Major processing steps in injection-molded ceramic manufacturing include preparation of ceramic powders and organic binders, mixing, molding, binder removal, sintering, and finishing [1]. While materials evaluation and diagnostics are needed throughout the process, it is particularly important to evaluate the distributions of binders/plasticizers in as-molded green bodies [2]. Poor distribution of these organics in a green body can lead to a final part that is defective or that has poor mechanical properties after it is sintered.

Magnetic resonance imaging (MRI), also called nuclear magnetic resonance (NMR) imaging, is a nondestructive/noninvasive evaluation method with the potential for providing extensive diagnostic information about spatial variations in the chemical and physical properties of ceramic materials. Notwithstanding the enormous impact of MRI in medical diagnosis [3], only limited studies have focused on materials applications [4,5]. This is mainly because of the inherently broad spectral linewidths and other complexities involved in imaging solid materials. Argonne National Laboratory has recently developed a solid-state MRI system for characterizing ceramic and polymeric materials [6]. It includes a special imaging probe capable of providing high gradient strengths (>50 G/cm), an advanced pulse programmer for

Review of Progress in Quantitative Nondestructive Evaluation, Vol. 10B
Edited by D.O. Thompson and D.E. Chimenti, Plenum Press, New York, 1991

experimental control, and a versatile set of image reconstruction software packages. Using this system, we evaluated proton (^1H) MRI techniques for quantitative measurement of the organic distributions in injection-molded green-state ceramics.

FABRICATION OF INJECTION-MOLDED TEST BARS

Injection-molded test bars for MRI tests were fabricated out of Si_3N_4 materials by the Garrett Ceramic Components Division [7]. The injection mixing and molding parameters were changed intentionally to introduce statistically different binder distributions for the tests. Table 1 presents the fabrication conditions for the test bars. Two combinations of mixes, prepared with standard and nonstandard procedures, were injection molded under two molding conditions, i.e., those using baseline and nonbaseline parameters. Thus, four different combinations of test bars were produced. In the nonstandard mixing procedure, mixing temperature and time were reduced significantly to upset the binder distribution. The nonbaseline molding condition consisted of changing the molding temperature, injection pressure, and injection speed from the baseline values.

NMR IMAGING OF TEST BARS

Four test bars, one in each combination with ID Nos. 1, 21, 41, and 69, were imaged with NMR. The ends of the bars were labeled gate end and nongate end, where gate end refers to the side where the material enters into the mold cavity. Because every bar is longer than the probe coil, each end of the bar was imaged separately, creating a total of eight NMR images. A small piece of injection-molded bar was used as the intensity standard, and was always placed next to the test bar to be imaged; this allowed normalization of the intensities of different images. Figure 1 shows the relative locations of the test bar and the intensity standard within the probe RF coil. Two-dimensional back-projection data were acquired in the x-z plane (along the width and length of the bars) by using the pulse sequence shown in Fig. 2 at a gradient strength of 3.6 G/cm. A total of 90 projections, each consisting of 128 averages per projection, were used to construct each image.

Table 1. Fabrication conditions of ceramic test bars used in imaging studies.

Bar Set	Test Bar I.D. No.	Mixing Procedure		Molding Parameter	
		Standard	Non-standard	Baseline	Non-baseline
A	1-4	X		X	
B	21-24		X	X	
C*	41-44		X		X
D*	69-72	X			X

*Exhibited a patchy pattern on the surfaces of all bars.

Figure 3 presents 2-D NMR images of each end of bars 1, 21, 41, and 69. Examine, for example, the images of the gate ends of bars 1 and 41. The image of bar 1 shows less uniformity in distribution of intensities than that of bar 41. This is rather surprising because bar 1 was produced under standard mixing and molding conditions, whereas bar 41 was produced under nonstandard conditions. To ensure that the void-like feature in the image of bar 1 is not an artifact, we repeated the experiment by moving the relative position of the bar up and down inside the RF coil; the defect was observed to move accordingly.

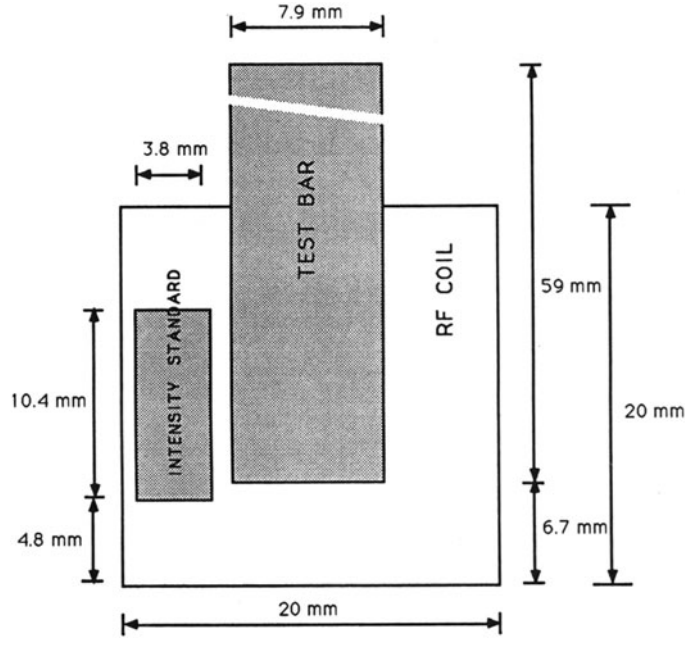

Fig. 1. Diagram of sample position within the probe RF coil.

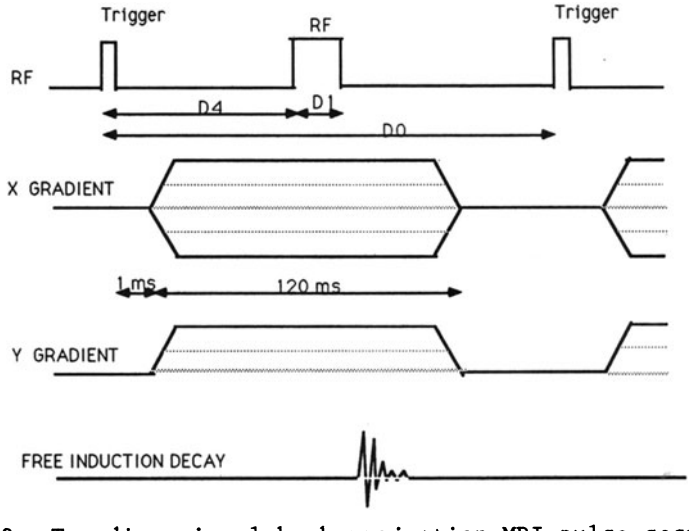

Fig. 2. Two-dimensional back-projection MRI pulse sequence (D0 = 0.5 s, D1=10 μs, and D4 = 85 ms).

We also made X-ray images of these bars to check for any ferromagnetic inclusions such as iron which would distort the MRI signals. The X-ray images showed some nonuniform density variations in the bars, but revealed no detectable features at the locations of interest. It is possible, however, that there may be minute paramagnetic inclusions that are below the detection level of X rays but that are within the sensitive range of MRI.

The images of the other bars contain no dominant features such as that seen in the image of bar 1. However, the images of bar 69 show less uniformity in intensity distribution than those of bars 41 or 21. There appears to be no significant differences between the images of the gate and nongate ends of the bars.

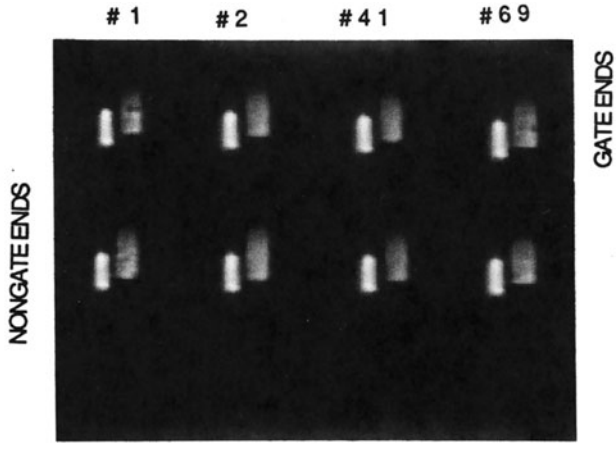

Fig. 3. Two-dimensional NMR images of Bars 1, 21, 41, and 69.

CORRELATION WITH DESTRUCTIVE TESTS

To determine the correlation between NMR image intensity and binder concentration in the test bars, a destructive evaluation was conducted. This involved cutting the bars (after imaging) into thin samples and then determining weight loss by thermogravimetric analysis (TGA). The bars were cut lengthwise; the thinnest sample possible was 2 mm thick, and any further sectioning across the width of the sample was not practical. A total of 54 samples were produced. These samples were heated in an air furnace to 650°C at 10°C/min, followed by a 2-h hold for binder removal. This thermal cycle was established on the basis of thermogravimetric analysis (TGA) data. The samples were weighed before and after thermal treatment with an analytical balance accurate to 0.0002 g, thus providing weight loss or percent of organic binders in each section.

The gray-scale image intensities of the test bars were analyzed for correlation with the gravimetric data of the organic binders. Using a PC-based image processing workstation, we selected areas of interest on the test bar images corresponding to the location and size of the sectioned samples. For each area of interest, the mean and standard deviations of the gray-scale intensities were obtained. In principle, the mean gray-scale intensity of a selected image area should be proportional to the percent weight of the organics in the corresponding sectioned sample. Before such direct comparisons can be made, however, the image data must be corrected for two known experimental variations or artifacts. One of these is due to a lack of absolute scaling in displayed NMR images, so a comparison between the test bar images requires scaling the images with respect to a reference. The other artifact is due to variation in probe response relative to sample location within the probe RF coil.

As was observed in our earlier concentration phantom experiments, the intensity standard was found to be unreliable for intensity scaling, perhaps due to changes in its orientation relative to the reference axis of the probe during sample mounting. Instead, the mean image intensity in the uniform field range of the probe was equated to the average weight of the organics in the corresponding section of the bar. Thus, we scaled the intensity values of all the images with respect to a reference weight.

The variation of probe response with respect to sample location can be eliminated if we restrict the image field of view to the uniform field region of the RF coil of the probe, which is about 0.7 times the radius of the coil from the center. But this would reduce the data points for correlation to a statistically insignificant number since the number of sectioned slices lying in the uniform field region is small. It is possible, however, to utilize the whole field of view if the probe response can be measured or predicted with respect to the sample position.

In this work, we predicted probe response by using half of the data points, i.e., the 27 data points corresponding to the nongate ends of the bars. Because probe response is desired for a uniform binder concentration, we weight-corrected the scaled image intensities to correspond to the reference weight chosen. Thus, we have 27 intensity values corresponding to different locations of a sample for a chosen reference weight. A fourth-degree polynomial fit of the data points was used to obtain the probe response function, which is given in Fig. 4. The center of the RF coil is 3.3 mm from the end of the bar, and the coil extends up to 13.3 mm in bar length. At first, probe response function shows an edge effect, which is an artifact of the image reconstruction technique. The uniform field region is up to ~ 9 mm long in the bar, after which the intensity decreases almost linearly with length. The scaled image intensities of the bars were thus corrected for the probe response variation.

Figure 5 is a representative plot of the MRI-predicted weights of the organics and the actual measured weights, with respect to distance from the gate end, for bar 21. A fairly good correlation between the MRI and gravimetric data is seen for all the test bars. To determine the overall correlation coefficient, we plotted all 57 pairs of data in the form of a scatter plot (Fig. 6). A linear regression of the data passing through the

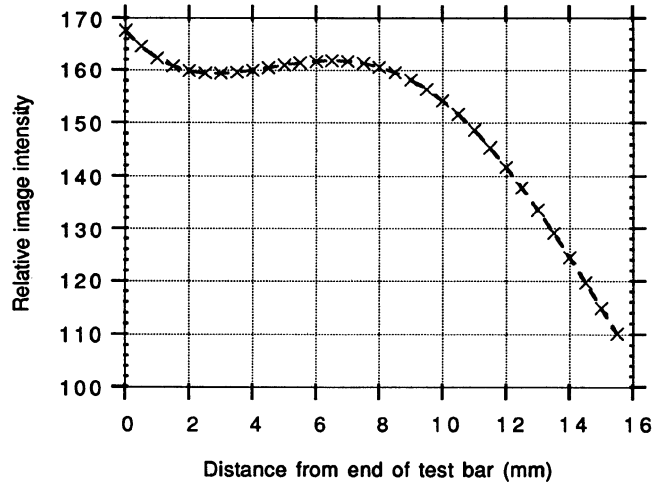

Fig. 4. Probe response function with respect to sample location.

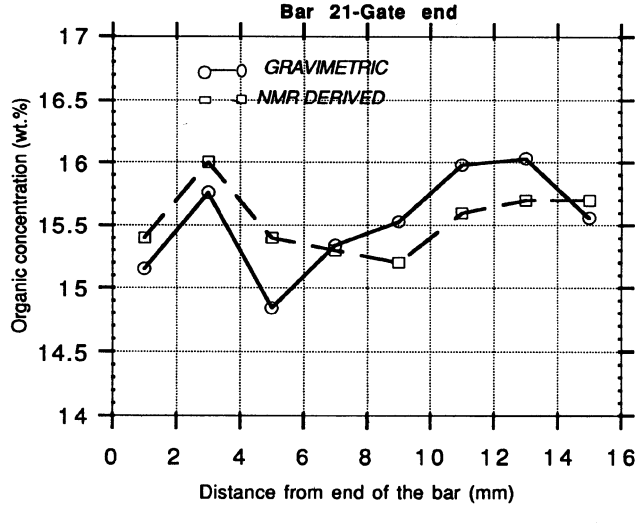

Fig. 5. Typical plot of organic concentrations as determined by gravimetric procedure (solid line) and NMR imaging (dashed line) for gate end of Bar 21.

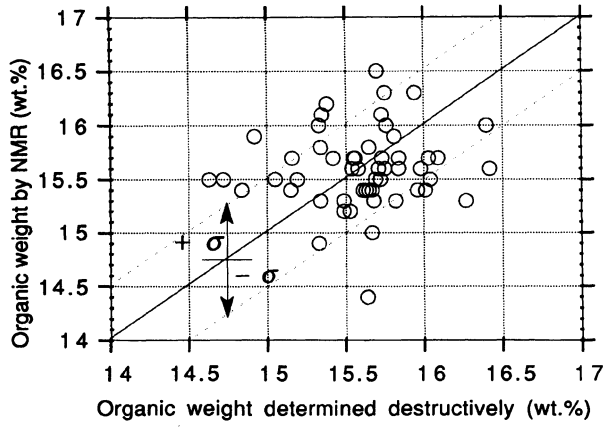

Fig. 6. Scatter plot of organic concentrations determined by gravimetric and NMR imaging methods.

origin was determined [8]. If the error bar for the regression fit is chosen at one standard deviation from the fitted line, the corresponding error in the MRI data is ±0.5 wt.%. For this case, 67% of the data are within the correlation band. Calculation of the correlation coefficient for the entire data set gives a value of about 0.1. The low correlation coefficient may be attributed to large measurement errors (poor signal-to-noise ratio) relative to the actual data spread. When the MRI data were taken, we were limited in the amount of RF power that could be transmitted to the probe coils because of a problem with capacitor arcing. As a result, the signal-to-noise ratios of the measurements were low. This problem has since been rectified, and we believe that our newer images would show higher correlation coefficients.

CONCLUSIONS

Magnetic resonance imaging (MRI) techniques were investigated for nondestructive evaluation of injection-molded structural ceramics. Several injection-molded Si_3N_4 test bars, fabricated with different mixing and molding parameters, were imaged by two-dimensional back-projection ^1H MRI techniques. The gray-scale intensities of the images were correlated with organic concentration data obtained by destructive testing. The correlation studies indicate that changes in the organic concentration to a level of ±0.5 wt.% can be detected with MRI. It is possible with these techniques to monitor the chemical changes that occur at various stages of ceramic processing and to use this information to improve ceramic processing and reliability.

ACKNOWLEDGMENTS

This work was supported by the U.S. Department of Energy, Assistant Secretary for Conservation and Renewal Energy, Office of Transportation Systems as part of the Ceramics Technology for Advanced Heat Engines Project of the Advanced Materials Development Program, under contract W-31-109-Eng-38.

REFERENCES

1. M. J. Edirisinghe and J. R. G. Evans, Materials Sci. Eng. A109, 17 (1989).

2. H. C. Yeh et al., Annual Technical Report to NASA by AiResearch Casting Co., Division of the Garrett Corporation, NASA-CR-175006 (1985).

3. P. Mansfield and P. G. Morris, NMR Imaging in Biomedicine, (Academic Press, New York, 1982).

4. W. A. Ellingson, P. S. Wong, S. L. Dieckman, J. L. Ackerman, and L. Garrido, The American Ceramic Society Bulletin, 68, 1180 (1989).

5. W. A. Ellingson, J. L. Ackerman, L. Garrido, J. Weyand, and R. A. DiMilia, Ceramic Eng. Sci. Proc. 8, 503 (1987).

6. N. Gopalsami, G. A. Forster, S. L. Dieckman, W. A. Ellingson, and R. E. Botto, in Review of Progress in Quantitative NDE, edited by D. O. Thompson and D. E. Chimenti (Plenum Press, New York, 1990), Vol. 9A, p. 861.

7. H. Yeh and J. Pollinger, Garrett Ceramic Components Division Report to Argonne National Laboratory (January 1990).

8. N. R. Draper and H. Smith, Applied Regression Analysis, (John Wiley, New York, 1966).